Published in final edited form as:
Biochemistry. 2011 April 5; 50(13): 2633–2641. doi:10.1021/bi200049c.

Phosphatidylinositol 4,5 bisphosphate alters Synaptotagmin 1 Membrane Docking and Drives Opposing Bilayers Closer Together†

Weiwei Kuo, **Dawn Z. Herrick**, and **David S. Cafiso***
Department of Chemistry and Center for Membrane Biology, University of Virginia, Charlottesville, VA, 22904-4319, USA

Abstract

Synaptotagmin 1 (syt1) is a synaptic vesicle-anchored membrane protein that acts as the calcium sensor for the synchronous component of neuronal exocytosis. Using site-directed spin labeling, the position and membrane interactions of a fragment of syt1 containing its two C2 domains (syt1C2AB) were determined in bilayers containing phosphatidylcholine (PC), phosphatidylserine (PS) and phosphatidylinositol, 4,5-bisphosphate (PIP_2). Addition of 1 mole% PIP_2 to a lipid mixture of PC and PS results in a deeper membrane penetration of the C2A domain and alters the orientation of the C2B domain so that the polybasic face of C2B comes into close proximity to the bilayer interface. The C2B domain is found to contact the membrane interface in two regions, the Ca^{2+}-binding loops and a region opposite the Ca^{2+}-binding loops. This suggests that syt1C2AB is configured to bridge two bilayers and is consistent with a model generated previously for syt1C2AB bound to membranes of PC and PS. Point-to-plane depth restraints, obtained by progressive power saturation, and interdomain distance restraints, obtained by double electron-electron resonance, were obtained in the presence of PIP_2 and used in a simulated annealing routine to dock syt1C2AB to two membrane interfaces. The results yield a different average structure than is found in the absence of PIP_2 and indicate that bilayer-bilayer spacing is decreased in the presence of PIP_2. The results indicate that PIP_2, which is necessary for bilayer fusion, alters C2 domain orientation, enhances syt1-membrane electrostatic interactions and acts to drive vesicle and cytoplasmic membrane surfaces closer together.

In the central nervous system, neurotransmitter release is mediated by a tightly regulated Ca^{2+}-triggered membrane fusion event. The SNARE[1] (soluble-N-ethylmaleimide-sensitive factor attachment protein receptor) proteins assemble into a stable four-helical bundle and are the central protein machinery that drives this fusion process (1–5). The prevailing model for SNARE activity, sometimes referred to as the SNARE hypothesis, proposes that the assembly and folding of the SNARE proteins (syntaxin, SNAP-25 and synaptobrevin) in an N-terminal to C-terminal direction drives fusion of the vesicle and plasma membranes (5).

†This work was supported by a grant from the National Institutes of Health, NIGMS, GM 072694.

*Correspondence should be addressed to David S. Cafiso, at the Department of Chemistry, McCormick Road University of Virginia, Charlottesville, VA 22904-4319, cafiso@virginia.edu, tel: 434-924-3067, fax 434-924-3567.

[1]Abbreviations used: DEER, double electron-electron resonance; EPR, electron paramagnetic resonance; MTSL, methanethiosulfonate spin label; PIP_2 or $PI4,5P_2$, phosphatidylinositol 4,5-bis phosphate; PC, phosphatidylcholine; POPC, palmitoyloleoylphosphatidylcholine; POPS, palmitoyloleoylphosphatidylserine; PS, phosphatidylserine; R1, spin-labeled side chain produced by derivatization of a cysteine with the MTSL; SDSL, site-directed spin labeling; SNARE, soluble-N-ethylmaleimide-sensitive factor attachment protein receptor; syt1, synaptotagmin 1; syt1C2AB, soluble fragment of syt1 containing the tandem C2A and C2B domains.

However, a number of other proteins regulate and are critical in this process, including CAPS, Munc18, complexin and synaptotagmin 1 (6,7).

In the neuronal system, there is strong evidence that Synaptotagmin 1 (syt1) acts as the Ca^{2+}-sensor for the synchronous component of exocytosis. A transmembrane helical segment anchors syt1 to the synaptic vesicle, and it contains two cytoplasmic C2 domains, termed C2A and C2B, that are C-terminal to the membrane anchor (Fig. 1). Both C2A and C2B bind Ca^{2+} and penetrate membranes containing negatively charged phospholipids in a Ca^{2+}-dependent manner (8–12). The C2B domain has a second weaker mode of binding to both PC:PIP_2 and PC:PS bilayers that is Ca^{2+}-independent (8,13). In addition to these membrane interactions, syt1 is also reported to interact with the SNARE complex (1,2,4,14); however, the structure of syt1 when associated with the SNARE complex does not appear to be well-defined and syt1 may sample multiple conformational substates when bound to SNAREs (15–17).

At the present time, the mechanism by which syt1 regulates membrane fusion has not been determined. Synaptotagmin 1 has been reported to alter membrane curvature, and this activity might promote the formation of a fusion stalk (18,19). The interactions of syt1 with the SNAREs could assist in driving SNARE assembly, or these interactions might promote SNARE folding from an intermediate meta-stable state (20). Synaptotagmin 1 also has the ability to bridge bilayers. Several studies indicate that syt1 aggregates vesicles in a Ca^{2+}-dependent manner (21,22), and depth and interdomain distance restraints obtained by site-directed spin labeling (SDSL) can only be satisfied if C2A and C2B align in an antiparallel manner so the C2A and C2B bind to opposing bilayers (23).

Electrostatic interactions play an important role in the membrane binding activity of syt1. For example, the Ca^{2+}-dependent membrane attachment of the syt1 C2A domain is mediated by Coulombic interactions with the negatively charged membrane surface, which are switched on when Ca^{2+} binds C2A (24). Coulombic interactions are also important in the membrane interactions of C2B, and the Ca^{2+}-independent binding of the C2B to membranes is mediated by a highly charged polybasic face on C2B (13). Two conserved arginine residues on C2B, which are located opposite the Ca^{2+}-binding face, appear to be critical for membrane fusion and the ability of C2B to aggregate lipid vesicles (25) and for the attachment of this region to the membrane interface (23).

The phosphorylated inositol lipid phosphatidylinositol 4,5-bis phosphate ($PI(4,5)P_2$ or PIP_2) is an essential signaling lipid that is required for membrane fusion (26,27). While PIP_2 levels average about 1 mol% in the plasma membrane (28), PIP_2 can reach levels of up 6 mol% at sites of active exocytosis in PC12 cells (29). Since PIP_2 has a valence of approximately $z=-4$ at neutral pH (30), PIP_2 likely makes a major contribution to the membrane charge density during exocytosis. Moreover, because of the high valence of this lipid, discreteness of charge effects become important and electrostatic interactions with proteins are enhanced relative to equivalent charge densities of monovalent lipids such as PS (30). As a result, relatively small levels of PIP_2 might be expected to have significant effects on the interactions made by the syt1 C2 domains with bilayers. There are reports that PIP_2 accelerates the membrane binding of the C2B domain and alters the membrane binding mode of C2B (8,12).

In the present study, we made use of SDSL to examine the effect of small levels of PIP_2 on the conformation of a fragment of syt1 containing its two C2 domains (syt1C2AB) when membrane associated in the presence of Ca^{2+}. A number of sites in syt1C2AB were derivatized with the spin labeled side-chain R1 (see Fig 1b), and a combination of continuous wave and pulse EPR were used to obtain bilayer depth restraints and interdomain

distance restraints when syt1C2AB is bound to PC:PS:PIP_2 bilayers. The results of a simulated annealing procedure using these restraints can only be satisfied if syt1C2AB bridges two bilayers, as was seen previously for membranes containing PC:PS (23). However, the addition of just 1 mol% PIP_2 to a PC:PS mixture enhances the electrostatic interaction between the C2B polybasic face and the membrane surface producing a change in the orientation of the C2B domain. The Ca^{2+}-binding face of C2A penetrates more deeply into the lipid interface, and the region opposite the Ca^{2+}-binding loops of C2B maintains contact with the bilayer interface. As a result, the model indicates that small levels of PIP_2 help drive opposing bilayers that are bridged by syt1 closer together. The implications of this PIP_2 mediated structural change in syt1 for membrane fusion are discussed.

Material and Methods

Mutagenesis, protein expression, and purification

For the cytosolic domain of rat syt1 C2A (96–265), C2B (249–421), and C2AB (96–421) cysteine mutants, the DNA modification, protein expression and purification were carried out as previously published (13,23). In brief, individual cysteine residues were introduced at positions in the tandem C2A, C2B, and C2AB domains using QuickChange Site-Directed Mutagenesis Kit (Stratagene, La Jolla, CA) or two-step PCR, following published protocols (31). All cysteine substitutions were confirmed by DNA sequencing. The mutants were expressed and purified with GST affinity and ion-exchange chromatography. For C2B and C2AB, the purity of protein was confirmed with UV spectrum to have the maximum absorption at 278 nm. The pure protein was treated with EDTA to ensure it was Ca^{2+}-free, and was lyophilized in NH_4HCO_3 and kept at −20 °C until it was labeled. Single-cysteine resides C2A 256, C2B 415 and C2AB 269 were used for vesicle sedimentation measurements; C2AB single cysteine mutants: 173, 174, 236, 283, 285, 304, 305, 306, 327, 368, 369, 395, and 396, and double cysteine mutants: 199/304, 199/332, 213/283 and 213/353 were used for EPR experiments.

Liposome preparations

1-Palmitoyl-2-oleoyl-sn-glycero-3-phosphatidycholine (POPC), 1-Palmitoyl-2-oleoyl-sn-glycero-3-phosphatidyserine (POPS), and L-α-phosphatidylinositol-4,5-bisphosphate (ammonium salt) (PIP_2) (Avanti Polar Lipids, Alabaster, AL) were used to prepare large unilamellar vesicles (POPC:POPS:PIP_2 74:25:1 or 70:25:5 molar %) with extrusion method. In order to produce evenly distributed PIP_2 membranes, extra caution was taken when preparing PIP_2 containing vesicles (32). Adequate amounts of POPC, POPS, and PIP_2 in chloroform were mixed in a 50-ml round-bottom flask, which was attached to a rotary evaporator and immersed in a 30–35 °C water bath. The flask was rotated without vacuum for 5 minutes and then slowly applied maximum vacuum to dry down the lipid mixture. Additional chloroform could be added and repeated the drying process to obtain an evenly coated lipid film on the flask. The resulting lipid film was vacuum desiccated overnight, rehydrated in either sucrose buffer (176 mM sucrose, 1 mM MOPS, pH 7.0) or EPR buffer (100 mM NaCl, 20 mM HEPES, pH 7.4), cycled through five freeze-thaw cycles, and extruded through 0.1-μm polycarbonate filters using a handheld Mini-Extruder (Avanti Polar Lipids, Alabaster, AL).

Fluorescence and spin labeling of syt1 C2 domains

Lyophilized syt1 C2A, C2B and C2AB domains were first brought up in EPR buffer or salt buffer (100 mM KCl, 20 mM MOPS, pH 7.0), then spin-labeled using methanethiosulfoate (MTSL, Toronto Research Chemicals, ON, Canada) at a 1:3:30 molar ratio of protein:DTT:MTSL, or fluorescence-labeled using Bodipy-FL C1-IA (Invitrogen, Carlsbad, CA) at a 1:8:10 molar ratio of protein:TCEP:Bodipy-FL. The excess spin and fluorescence

labels were removed with HiPrep desalting column (GE Healthcare, Piscataway, NJ). The labeled protein was concentrated to 20–300 μM using an Amicon micro concentrator (Millipore, Billerica, MA). Spin-labeled protein was stored in EPR buffer where it was in a Ca^{2+}-free state. For sedimentation assays under a Ca^{2+}-free conditions, an additional 1 mM EGTA was added to the protein samples. Additional $CaCl_2$ (1 mM final concentration) was added in the samples for Ca^{2+} condition in EPR study.

EPR spectroscopy

EPR spectra were recorded at room temperature using a Varian E-line Century series spectrometer fitted with a microwave preamplifier and a X-band loop gap resonator (Medical Advances, Milwaukee, WI). 20–300 μM of aqueous syt1 protein was mixed with POPC:POPS:PIP_2 (75:25:1) LUVs (25 mM total lipid) for membrane-associated spectra. Continuous wave power saturation experiments were performed using Bruker EMX spectrometer with a dielectric resonator and results were used to calculate a depth parameter, Φ, based upon the saturation behavior in the samples containing oxygen and 10 mM Ni(II)EDDA. $\Delta P_{1/2}$ values of Ni(II)EDDA was scaled to an effective concentration of 20 mM. Distances were calculated based on Equation 1 which obtained previously describing the correlation of distance (x) and Φ values (33).

$$\Phi = 3.4 \tanh[0.11(x - 8.56)] + 1.1 \quad \text{Eq. 1}$$

Depth measurements using a collision gradient approach may vary with lipid composition, and the validity Eq. 1 for POPC:POPS mixtures containing low levels of PIP_2 was tested by measuring Φ for spin-labeled lipids in the presence and absence of 1 mol% PIP_2. Incorporation of PIP_2 at this low level in POPC:POPS had no measurable effect on Φ and did not alter the either oxygen or Ni(II)EDDA $\Delta P_{1/2}$ values.

Pulse-EPR measurements and sample preparation were published previously (23). In brief, 25–30 μl double-labeled protein sample with presence of 1 mM Ca^{2+}, POPC:POPS:PIP_2 (74:25:1) vesicles and 10–20% v/v glycerol were loaded into quartz capillaries. Samples were flash frozen in a dry ice/isopropanol bath, and the data were recorded at 80K on a Bruker Elexsys E580 spectrometer fitted with an ER4118X-MS3 split-ring resonator (Bruker Biospin, Billerica, MA). The phase-corrected dipolar evolution data were processed assuming a 3D background and Fourier transformed, and the distance distributions were obtained with a Gaussian fit using DeerAnalysis2009 package.

Vesicle sedimentation assay

Vesicle sedimentation assays were carried out as described previously (34) and free protein concentrations were determined from the fluorescence of a Bodipy-labeled protein or the intrinsic fluorescence of native protein. Here, experiments were carried out with 0.1–0.5 μM of Bodipy- labeled C2A protein, ~10 nM for C2B and ~ 1 μM of unlabeled C2AB 269. Additional 1 mM $CaCl_2$ or 1 mM EGTA was added in Ca^{2+} - bound and Ca^{2+} -free conditions with sucrose-loaded LUVs at lipid concentrations ranging from 1 μM to 12 mM. Final lipid concentration was confirmed with phosphate assay (35). The emission spectrum taken with FluoroMax-3 fluorimeter (Jobin Yvon, Edison, NJ) with excitation at 480 nm and emission intensity at 510 nm was measured for binding calculation of C2A and C2AB; tryptophan fluorescence of C2AB was recorded with excitation at 290 nm and emission at 342 nm. At least three set of measurements were made for each lipid concentration and used to determine a molar partition coefficient, K, which is defined as:

$$\frac{[P]_m}{[L]} = K[P] \quad \text{Eq. 2}$$

[P] is the concentration of protein in the bulk aqueous phase, $[P]_m$ is the molar concentration of protein bound to the membrane, and [L] is the molar concentration of accessible lipid. Here, the protein concentrations are dilute ([lipid] ≫ [protein]), so the fraction of protein bound, f_b, will be given by:

$$f_b = \frac{K[L]}{1+K[L]} \quad \text{Eq. 3}$$

The data were fit to Eq. 2 using OriginPro 7.5 to yield a value of K, the reciprocal molar partition coefficient with units of M^{-1}.

Modeling the membrane docking of the syt 1 C2AB domain

Models for the membrane-bound structure of syt1C2AB were generated in a similar manner to that described previously (23). Briefly, the spin-label side chain R1 was appended to the structure at appropriate locations and the first two dihedral angles for the side chain, χ_1 and χ_2, were set to −60°. A simulated annealing routine was performed without any experimental restraints to allow other side-chain atoms to find reasonable conformations. The result of this procedure was the starting structure for the membrane docking simulation during which the entire spin-label side-chain conformations were fixed in addition to the backbone atoms of the two C2 domains. The distances of which R1 side chains (at positions of C2AB 173, 174, 236, 283, 285, 304, 305, 306, 327, 368, 369,395, and 396) relative to the membrane surface were calculated from the experimentally determined Φ values as described previously (13). Simulated annealing was performed with restraints based on power saturation (distances to plane) and DEER (inter-domain distances, 199–304, 199–332, 213–283, and 213–353). Structures were visualized and analyzed with the program PyMOL (DeLano Scientific LLC, Palo Alto, CA). Average structure angles and distances were measured with the program Discovery Studio Visualizer 2.5 (Accelrys, San Diego, CA).

Electrostatic Calculations of the syt1 C2B domain

The Adaptive Poisson-Boltzmann Solver (APBS) plug-in (36) within PyMOL was used to calculate electrostatic potential maps on the NMR solution structure of C2B (PDB ID: 1K5W) (37). The Ca^{2+}-bound C2B electrostatic profile was determined with the radius of the two Ca^{2+} ions set to 1.06 Å (38). Protein and solvent dielectric constants were set to 2 and 78, respectively. A graphical representation of the calculated electrostatic potential isocontours in 150 mM monovalent ions at 1kT/e (approximately 25 mV) was displayed using PyMOL.

Results

1% PI(4,5)P_2 alters the orientation of and depth of penetration of syt 1C2AB

The spin labeled side chain R1 was incorporated into the soluble fragment of syt1 containing its two C2 domains (syt1C2AB) at 13 different positions by derivatizing a single cysteine mutant with the MTSL reagent (Fig. 1). Most of these positions were chosen for labeling because the R1 label was seen previously to penetrate POPC:POPS bilayers, or because the EPR spectra of R1 exhibited changes upon membrane association. Shown in Figure 2 are the X-band EPR spectra of these single R1 mutants when fully associated with either

POPC:POPS (3:1) or POPC:POPS:PIP_2 (74:25:1) in the presence of Ca^{2+} (black and red traces, respectively). The lineshapes at each site are a reflection of the local structure at each labeled position as well as the penetration of the label into the membrane hydrocarbon (10). For most sites, no significant differences in the EPR spectra are seen, indicating that the label motion at these sites is unchanged by the presence of 1 mol% PIP_2. However, there are small but significant differences in the spectra at several sites, including the Ca^{2+}-binding loops of C2A as well as Ca^{2+}-binding loop 3 of C2B. These changes might reflect a different membrane association of syt1C2AB in the presence of PIP_2.

To determine whether changes in the EPR spectra reflect a difference in association of syt1C2AB to the bilayer, each of the spectra in Fig. 2 were power-saturated to obtain a measure of the depth of membrane penetration of each label (see Methods). The depth parameters obtained in the presence of PIP_2 are shown in Table 1, along with depth parameters obtained previously for syt1C2AB associated with POPC:POPS (23). As seen in Table 1, PIP_2 induces a deeper membrane penetration (more positive depth parameters) for sites in the Ca^{2+}-binding loops of C2A (173R1, 174R1, 236R1), and PIP_2 alters the positions of labels within Ca^{2+}-binding loops of C2B (304R1, 305R1, 368R1, 369R1). In addition, a site within the polybasic strand (327R1) moves closer to the membrane interface in the presence of PIP_2 and several sites opposite the Ca^{2+}-binding loops in C2B (396R1 and 285R1) reside at the membrane interface.

Increasing the PIP_2 concentration brings the polybasic face of C2B closer to the bilayer interface

Levels of PIP_2 up to 6 mol% have been detected at the focal sites of fusion, and we explored the effect of increasing the PIP_2 concentration from 1 to 5 mol%. In most cases, further increases in PIP_2 do not significantly change lineshapes (see Fig. 3a) or depth parameters; however, EPR lineshapes broaden for residues within the highly charged polybasic face of C2B, for example at 327R1. For 327R1 increasing the PIP_2 concentration from 1 to 5 mol% increases the depth parameter, Φ, from −1.7 (±0.1) to −1.1 (±0.1), representing a shift in position towards the bilayer of approximately 3 Å. This is not unexpected. The incorporation of 5 mol% PIP_2 represents a significant increase in the membrane surface charge density, and increases in charge density are known to alter the equilibrium position of peptides that interact electrostatically with the membrane interface (39).

PIP_2 enhances the Ca^{2+}-independent binding of Syt1C2AB

Previously, syt1 C2AB was shown to interact with POPC:POPS bilayers in a Ca^{2+}-independent manner through the electrostatic association of the polybasic face of C2B with the bilayer interface (13). Although this association is weak, the C2B domain will remain membrane associated within the cell (if it is not associated with SNARE proteins) because it is tethered to the bilayer interface thereby increasing the local lipid concentration. A well-established vesicle sedimentation assay was used to determine the partition coefficients for the C2A, C2B, and C2AB fragments of syt1 to the bilayer interface under conditions where the protein is dilute on the membrane interface. The binding data are shown in Fig. 4 along with fits to the data using Eq. 3. There was no measurable affinity of the C2A domain to bilayers composed of POPC:POPS:PIP_2 bilayers in the absence of Ca^{2+}. The reciprocal molar partition coefficients for C2B and C2AB obtained from the fits in Fig. 4 are shown in Table 2. In the presence of PIP_2, syt1C2B and syt1C2AB have a similar bilayer affinity, and the domains will be half membrane bound at an accessible lipid concentration of approximately 1 mM. The values obtained previously in POPC:POPS are shown for comparison and indicate that addition of 1 mol% PIP_2 to POPC:POPS bilayers produces approximately 3 fold and 8 fold increases in membrane affinity for C2B and C2AB, respectively.

The incorporation of PIP_2 does not significantly change most EPR lineshapes for membrane associated syt1C2AB in the absence of Ca^{2+}, except within the first Ca^{2+}-binding loop of C2B (see Fig. 3b). For these sites, membrane depth parameters indicate that the first Ca^{2+}-binding loop is positioned closer to the interface. For example, the depth parameter for 304R1 increases from −1.3±0.1 without PIP_2 to −0.5±0.4 in the presence of 1% PIP_2, indicating a shift into the interface of about 4 Å.

Syt1C2AB bridges bilayers and 1% PIP_2 drives bilayers closer together

The data shown in Table 1 provide point-to-plane depth restraints that may be used to determine the membrane docking of syt1C2AB. To provide additional structural restraints, four distances were measured across the two C2 domains of syt1 when fully bound to membranes containing PIP_2. Shown in Fig. 5a are positions in syt1C2AB from which the interdomain restraints were measured. Also shown in Fig. 5 are the background-corrected DEER signal and Pake pattern obtained for the nitroxide pair 199R1/304R1. The signals obtained from 199R1/304R1 are similar to the three other signals, and they resemble those obtained previously in POPC:POPS (23). These DEER signals result from a broad distance distribution between nitroxide pairs, and in the present case they reflect structural heterogeneity in the relative orientations of C2A and C2B. The distances obtained by pulse EPR are shown in Table 3, and they represent the most probable distance and one standard deviation of the width of the Gaussian used to fit the distance distribution. Each of the distances measured has a broad distribution and was similar to interdomain distances obtained for syt1C2AB bound to PC:PS bilayers.

Using the structural restraints shown in Table 1 and Table 3, we generated a model for the membrane bound form of syt1C2AB using an approach that was employed previously to dock syt1C2AB to PC:PS bilayers. Using these restraints, it was not possible to dock the two C2 domains of syt1 to a single bilayer (a result that was obtained previously using restraints generated in POPC:POPS (23)). However, the restraints could be satisfied by docking syt1C2AB to two bilayers, and the result is shown in Fig. 6.

In the model shown in Fig. 6, the first and third Ca^{2+}-binding loops of C2A and C2B penetrate into opposite bilayers. The polybasic face of C2B, which includes a number of basic residues along its fourth β-strand, is closely associated with one interface, and the region opposite the Ca^{2+}-binding loops of C2B also interacts with the bilayer interface. This interaction includes the pair of conserved residues, Arg 398 and Arg 399, which likely promote association with the POPC:POPS:PIP_2 bilayer.

In Fig. 7 the model obtained here for syt1 bound to bilayers containing 1 mol% PIP_2 is compared with a model obtained previously in POPC:POPS (23). In the presence of PIP_2, both domains penetrate more deeply into the bilayer through their Ca^{2+}-binding loops, with loop 3 of C2B penetrating about 6 Å deeper in the presence of PIP_2. In addition, the polybasic face of C2B is drawn closer to the bilayer interface in the presence of PIP_2, which tilts the axis of C2B further from the bilayer normal. Because the C2B domain bridges bilayers and retains bilayer contact on two faces, the separation between bilayers that best satisfies the restraints in the presence of PIP_2 is shorter than that obtained without PIP_2. In the presence of PIP_2, the optimal separation between bilayers that produces structures with the lowest energy and with a minimum in the number of violations is approximately 35 Å; whereas in the absence of PIP_2, the optimal separation was approximately 43 Å. Based upon the error in the depth measurements and the variation in structures obtained from the simulated annealing, we estimate that the 8 Å decrease in distance has an error of approximately +/− 3 Å.

It should be noted that the structures shown in Fig. 6 and Fig. 7 represent the lowest energy structures obtained from a set of structures obtained by simulated annealing. Caution needs to be taken when interpreting any one structure, as there is considerable variability in the structures obtained (the RMSD of the ten lowest energy structures obtained in the presence of 1 mol% PIP_2 was 3.77 +/− 1.25 Å). Nonetheless, the results indicate that PIP_2, mediated by electrostatic interactions with syt1C2AB, acts to bring two opposing bilayers closer together.

Discussion

At the present time, the role of PIP_2 in membrane fusion is not understood. PIP_2 is known to play an important role in cell-signaling, functioning as a precursor to cellular second messengers and acting as a signaling lipid itself. At a molecular level, PIP_2 frequently acts to bind and translocate proteins containing specific domains, such as PH domains, to the membrane surface (40), and it is known to facilitate the attachment of positively charged segments of proteins to the membrane interface through electrostatic interactions (41). Moreover, basic protein motifs have the capacity to sequester PIP_2, thereby regulating the lateral distribution and activity PIP_2 within the bilayer. Indeed, there is evidence that the highly charged juxta-membrane region of syntaxin interacts with PIP_2 and controls the activity of this lipid within the focal site of fusion (29). Since PIP_2 has a high-positive intrinsic curvature, it should be highly inhibitory to fusion when present on cytoplasmically facing target monolayer. As a result, it has been suggested that PIP_2 might act to prevent fusion until it is removed during the final triggering step for exocytosis. There is also evidence that PIP_2 plays a direct role in fusion by helping bridge bilayers through electrostatic interactions with the positively charged juxta-membrane segment of the vesicle SNARE synaptobrevin (42).

In the present work, we utilized both pulse and continuous wave EPR spectroscopy to generate a model for syt1C2AB when bound to POPC:POPS bilayers containing 1 mol% PIP_2. The model suggests that PIP_2 modulates the configuration of syt1 and may act to decrease the spacing between bilayers at the focal site of fusion. In this model, the Ca^{2+}-binding loops of the C2 domains of syt1 penetrate more deeply into bilayers in the presence of PIP_2 and the orientation of the C2B domain changes to bring the polybasic face of this domain closer to the membrane interface. The restraints obtained here indicate that the C2B domain of syt1 must bridge bilayers, and the results of simulated annealing indicate that the most likely configurations are those where the C2A and C2B domains bind opposing bilayers. Because the C2B domain bridges bilayers, the change in orientation of C2B results in a shorter distance between the two opposing bilayers.

The model shown in Fig. 6 and Fig. 7b, was obtained for syt1C2AB bound to bilayers that both contain 1 mol% PIP_2. In the cell, the majority of the PIP_2 is believed to be present on the plasma membrane interface and not the vesicle interface (29), and unlike this experimental system, the native system is not symmetric. Although we have no data for an asymmetric system, the two C2 domains have different Ca^{2+}-dependent lipid preferences, with the C2B domain preferring to associate with PIP_2 containing bilayers and the C2A domain preferring PS containing bilayers (8). As a result, the calcium binding loops of C2A and C2B would be predicted to associate with the vesicle and plasma membranes, respectively. The presence of PIP_2 in the target membrane is expected to have a similar effect to that seen in our model system. The presence of PIP_2 on the plasma membrane surface should enhance interactions with the polybasic face of C2B, alter the C2B domain orientation and decrease bilayer separation.

The C2B domain is a highly charged protein domain, and electrostatic surface potential plots (showing the +25 mV and −25 mV equipotential surfaces) for the C2B domain in Ca^{2+}-free and Ca^{2+}-bound forms are shown in Fig. 8. The addition of Ca^{2+} creates a region of positive electrostatic potential around the Ca^{2+}-binding loops of C2B and the polarization of this region likely triggers C2B domain insertion into lipid bilayers in a manner similar to that for the C2A domain (24). Even in the absence of Ca^{2+}, the C2B domain is highly positively charged, with regions of large positive surface potential near the polybasic face and the region opposite the Ca^{2+}-binding loops. These electrostatic features likely mediate the change in orientation of the C2B domain in the presence of PIP_2 and the membrane contact that is observed in a region opposite the Ca^{2+}-binding loops (see Fig. 6) (23). Two conserved basic residues opposite the Ca^{2+}-binding loops of on C2B, Arg 398 and Arg 399 (Fig. 6 and Fig. 8) make a significant contribution to the positive electrostatic potential on this end of the domain, and they are also functionally important. When these residues are mutated to glutamine, Ca^{2+}-trigged synchronous release is nearly abolished (25).

The model shown in Fig. 6 seems physically plausible. The two opposing bilayers are both negatively charged; however, strong electrostatic repulsion should not take place since the separation between bilayers is greater than twice the Debye length at normal ionic strength. As indicated above, the C2B domain is highly positively charged and as a result, syt1 acts as an electrostatic mediator to bring the two bilayers closer together. The changes seen here in C2 domain orientation with PIP_2 addition are not unexpected, since previous work provided qualitative evidence for changes in C2B domain orientation in the presence of PIP_2 (8,12). PIP_2 has been observed to modulate the binding and orientation of the C2 domain of PKCα (43); however, in this case the domain is tilted towards the bilayer normal in the presence of PIP_2. The different behavior of the syt1 and PKC domains appears to be due to differences in the PIP_2 interacting face of these domains. Unlike the syt1 C2B domain, which likely responds to PIP_2 through a purely electrostatic mechanism, the behavior of the PKCα C2 domain appears to be due to a specific binding site for the PIP_2 headgroup on the domain (44).

Evidence for bilayer bridging by syt1C2AB has been observed previously and it could play an important role in syt1 function. As indicated above, a model generated previously in POPC:POPS (using 21 point-to-plane and 12 interdomain distance restraints), places syt1C2AB in a configuration to bridge bilayers (Fig. 7a). Moreover, light scattering and electron microscopy both indicate that syt1C2AB aggregates vesicles in a Ca^{2+}-dependent fashion (21,22). Evidence for bilayer bridging also comes from functional assays of syt1 function. Recently, fusion in a Ca^{2+}-dependent manner mediated by syt1 has been demonstrated using full-length syt1 and a single vesicle fusion assay (45). In this case, high PIP_2 levels were required in the target membrane for optimal Ca^{2+}-sensitivity, suggesting that a trans-bilayer interaction of syt1 was required to stimulate fusion. This work is consistent with earlier work in a bulk vesicle fusion assay, indicating that trans-bilayer interactions of syt1 were likely to mediate fusion (46).

In summary, the work carried out here indicates that PIP_2, by changing the membrane position and orientation of syt1, acts to drive vesicle and target membranes closer together. How might membrane bridging or trans-bilayer interactions of syt1 mediate synchronous Ca^{2+}-dependent neurotransmitter release? Conceivably, this bridging activity might act to trigger the assembly and zippering of the SNARE complex from either a disassembled or partially assembled state. Bilayer bridging might also act to promote the mixing of lipids in the two opposing bilayers and the formation of a fusion stalk. It has been proposed that syt1 acts by altering lipid order or curvature strain (19), thereby promoting the formation of a fusion stalk. Conceivably, the deeper penetration of the C2 domains and the presence of

PIP_2, which may be sequestered near the focal site of fusion, could act to amplify the local positive membrane curvature strain near the site of fusion.

Acknowledgments

We would like to thank Christian Altenbach (UCLA) for providing LabVIEW programs used to process and simulate EPR spectra. We also acknowledge helpful discussions with Jeff Ellena and Lukas Tamm (University of Virginia) and Reinhard Jahn (Max-Plank-Institute Göttingen, Germany).

References

1. Sudhof TC. The synaptic vesicle cycle. Annual review of neuroscience. 2004; 27:509–547.
2. Chapman ER. How does synaptotagmin trigger neurotransmitter release? Annu Rev Biochem. 2008; 77:615–641. [PubMed: 18275379]
3. Rothman JE. Intracellular membrane fusion. Adv Second Messenger Phosphoprotein Res. 1994; 29:81–96. [PubMed: 7848733]
4. Rizo J, Chen X, Arac D. Unraveling the mechanisms of synaptotagmin and SNARE function in neurotransmitter release. Trends Cell Biol. 2006; 16:339–350. [PubMed: 16698267]
5. Jahn R, Scheller RH. SNAREs--engines for membrane fusion. Nature reviews. 2006; 7:631–643.
6. James DJ, Kowalchyk J, Daily N, Petrie M, Martin TF. CAPS drives trans-SNARE complex formation and membrane fusion through syntaxin interactions. Proc Natl Acad Sci U S A. 2009; 106:17308–17313. [PubMed: 19805029]
7. Rizo J, Rosenmund C. Synaptic vesicle fusion. Nat Struct Mol Biol. 2008; 15:665–674. [PubMed: 18618940]
8. Bai J, Tucker WC, Chapman ER. PIP2 increases the speed of response of synaptotagmin and steers its membrane-penetration activity toward the plasma membrane. Nat Struct Mol Biol. 2004; 11:36–44. [PubMed: 14718921]
9. Bai J, Chapman ER. The C2 domains of synaptotagmin--partners in exocytosis. Trends Biochem Sci. 2004; 29:143–151. [PubMed: 15003272]
10. Frazier AA, Roller CR, Havelka JJ, Hinderliter A, Cafiso DS. Membrane-bound orientation and position of the synaptotagmin I C2A domain by site-directed spin labeling. Biochemistry. 2003; 42:96–105. [PubMed: 12515543]
11. Herrick DZ, Sterbling S, Rasch KA, Hinderliter A, Cafiso DS. Position of synaptotagmin I at the membrane interface: cooperative interactions of tandem C2 domains. Biochemistry. 2006; 45:9668–9674. [PubMed: 16893168]
12. Rufener E, Frazier AA, Wieser CM, Hinderliter A, Cafiso DS. Membrane-bound orientation and position of the synaptotagmin C2B domain determined by site-directed spin labeling. Biochemistry. 2005; 44:18–28. [PubMed: 15628842]
13. Kuo W, Herrick DZ, Ellena JF, Cafiso DS. The calcium-dependent and calcium-independent membrane binding of synaptotagmin 1: two modes of C2B binding. J Mol Biol. 2009; 387:284–294. [PubMed: 19302798]
14. Brunger AT. Structure and function of SNARE and SNARE-interacting proteins. Quarterly reviews of biophysics. 2005; 38:1–47. [PubMed: 16336742]
15. Dai H, Shen N, Arac D, Rizo J. A quaternary SNARE-synaptotagmin-Ca2+-phospholipid complex in neurotransmitter release. J Mol Biol. 2007; 367:848–863. [PubMed: 17320903]
16. Choi UB, Strop P, Vrljic M, Chu S, Brunger AT, Weninger KR. Single-molecule FRET-derived model of the synaptotagmin 1-SNARE fusion complex. Nat Struct Mol Biol. 2010; 17:318–324. [PubMed: 20173763]
17. Lai AL, Huang H, Herrick DZ, Epp N, Cafiso DS. Synaptotagmin 1 and SNAREs Form a Complex That Is Structurally Heterogeneous. J Mol Biol. 2011; 405:696–706. [PubMed: 21087613]
18. Martens S, Kozlov MM, McMahon HT. How synaptotagmin promotes membrane fusion. Science. 2007; 316:1205–1208. [PubMed: 17478680]

19. McMahon HT, Kozlov MM, Martens S. Membrane curvature in synaptic vesicle fusion and beyond. Cell. 2010; 140:601–605. [PubMed: 20211126]
20. Sorensen JB. Conflicting views on the membrane fusion machinery and the fusion pore. Annu Rev Cell Dev Biol. 2009; 25:513–537. [PubMed: 19575641]
21. Arac D, Chen X, Khant HA, Ubach J, Ludtke SJ, Kikkawa M, Johnson AE, Chiu W, Sudhof TC, Rizo J. Close membrane-membrane proximity induced by Ca(2+)-dependent multivalent binding of synaptotagmin-1 to phospholipids. Nat Struct Mol Biol. 2006; 13:209–217. [PubMed: 16491093]
22. Connell E, Giniatullina A, Lai-Kee-Him J, Tavare R, Ferrari E, Roseman A, Cojoc D, Brisson AR, Davletov B. Cross-linking of phospholipid membranes is a conserved property of calcium-sensitive synaptotagmins. J Mol Biol. 2008; 380:42–50. [PubMed: 18508081]
23. Herrick DZ, Kuo W, Huang H, Schwieters CD, Ellena JF, Cafiso DS. Solution and membrane-bound conformations of the tandem C2A and C2B domains of synaptotagmin 1: Evidence for bilayer bridging. J Mol Biol. 2009; 390:913–923. [PubMed: 19501597]
24. Murray D, Honig B. Electrostatic control of the membrane targeting of C2 domains. Mol Cell. 2002; 9:145–154. [PubMed: 11804593]
25. Xue M, Ma C, Craig TK, Rosenmund C, Rizo J. The Janus-faced nature of the C(2)B domain is fundamental for synaptotagmin-1 function. Nat Struct Mol Biol. 2008; 15:1160–1168. [PubMed: 18953334]
26. Martin TF. Stages of regulated exocytosis. Trends Cell Biol. 1997; 7:271–276. [PubMed: 17708959]
27. Martin TF. PI(4,5)P(2) regulation of surface membrane traffic. Curr Opin Cell Biol. 2001; 13:493–499. [PubMed: 11454457]
28. Takamori S, Holt M, Stenius K, Lemke EA, Gronborg M, Riedel D, Urlaub H, Schenck S, Brugger B, Ringler P, Muller SA, Rammner B, Grater F, Hub JS, De Groot BL, Mieskes G, Moriyama Y, Klingauf J, Grubmuller H, Heuser J, Wieland F, Jahn R. Molecular anatomy of a trafficking organelle. Cell. 2006; 127:831–846. [PubMed: 17110340]
29. James DJ, Khodthong C, Kowalchyk JA, Martin TF. Phosphatidylinositol 4,5-bisphosphate regulates SNARE-dependent membrane fusion. J Cell Biol. 2008; 182:355–366. [PubMed: 18644890]
30. McLaughlin S, Murray D. Plasma membrane phosphoinositide organization by protein electrostatics. Nature. 2005; 438:605–611. [PubMed: 16319880]
31. Sambrook, J.; Fritsch, EF.; Maniatis, T. Molecular Cloning: A Laboratory Manual. Plainview, N.Y: Cold Spring Harbor Press; 1989.
32. Wang J, Gambhir A, Hangyas-Mihalyne G, Murray D, Golebiewska U, McLaughlin S. Lateral sequestration of phosphatidylinositol 4,5-bisphosphate by the basic effector domain of myristoylated alanine-rich C kinase substrate is due to nonspecific electrostatic interactions. J Biol Chem. 2002; 277:34401–34412. [PubMed: 12097325]
33. Frazier AA, Wisner MA, Malmberg NJ, Victor KG, Fanucci GE, Nalefski EA, Falke JJ, Cafiso DS. Membrane orientation and position of the C2 domain from cPLA2 by site-directed spin labeling. Biochemistry. 2002; 41:6282–6292. [PubMed: 12009889]
34. Buser CA, McLaughlin S. Ultracentrifugation technique for measuring the binding of peptides and proteins to sucrose-loaded phospholipid vesicles. Methods Mol Biol. 1998; 84:267–281. [PubMed: 9666456]
35. Ames, BN. Assay of inorganic phosphate, total phosphate and phosphatases. In: Neufeld, EF.; Ginsburg, V., editors. Methods in Enzymology. Academic Press; 1966. p. 115-118.
36. Baker NA, Sept D, Joseph S, Holst MJ, McCammon JA. Electrostatics of nanosystems: Application to microtubules and the ribosome. Proceedings of the National Academy of Sciences of the United States of America. 2001; 98:10037–10041. [PubMed: 11517324]
37. Fernandez I, Araç D, Ubach J, Gerber SH, Shin O-h, Gao Y, Anderson RGW, Südhof TC, Rizo J. Three-Dimensional Structure of the Synaptotagmin 1 C2B-Domain: Synaptotagmin 1 as a Phospholipid Binding Machine. Neuron. 2001; 32:1057–1069. [PubMed: 11754837]
38. Falke JJ, Drake SK, Hazard AL, Peersen OB. Molecular Tuning of Ion Binding to Calcium Signaling Proteins. Quarterly reviews of biophysics. 1994; 27:219–290. [PubMed: 7899550]

39. Qin Z, Cafiso DS. Membrane structure of protein kinase C and calmodulin binding domain of myristoylated alanine rich C kinase substrate determined by site-directed spin labeling. Biochemistry. 1996; 35:2917–2925. [PubMed: 8608129]
40. Overduin M, Cheever ML, Kutateladze TG. Signaling with phosphoinositides: better than binary. Mol Interv. 2001; 1:150–159. [PubMed: 14993348]
41. McLaughlin S, Wang J, Gambhir A, Murray D. PIP(2) and proteins: interactions, organization, and information flow. Annu Rev Biophys Biomol Struct. 2002; 31:151–175. [PubMed: 11988466]
42. Williams D, Vicogne J, Zaitseva I, McLaughlin S, Pessin JE. Evidence that electrostatic interactions between vesicle-associated membrane protein 2 and acidic phospholipids may modulate the fusion of transport vesicles with the plasma membrane. Mol Biol Cell. 2009; 20:4910–4919. [PubMed: 19812247]
43. Landgraf KE, Malmberg NJ, Falke JJ. Effect of PIP2 binding on the membrane docking geometry of PKC alpha C2 domain: an EPR site-directed spin-labeling and relaxation study. Biochemistry. 2008; 47:8301–8316. [PubMed: 18610985]
44. Guerrero-Valero M, Ferrer-Orta C, Querol-Audi J, Marin-Vicente C, Fita I, Gomez-Fernandez JC, Verdaguer N, Corbalan-Garcia S. Structural and mechanistic insights into the association of PKCalpha-C2 domain to PtdIns(4,5)P2. Proc Natl Acad Sci U S A. 2009; 106:6603–6607. [PubMed: 19346474]
45. Lee HK, Yang Y, Su Z, Hyeon C, Lee TS, Lee HW, Kweon DH, Shin YK, Yoon TY. Dynamic Ca2+-dependent stimulation of vesicle fusion by membrane-anchored synaptotagmin 1. Science. 2010; 328:760–763. [PubMed: 20448186]
46. Stein A, Radhakrishnan A, Riedel D, Fasshauer D, Jahn R. Synaptotagmin activates membrane fusion through a Ca2+-dependent trans interaction with phospholipids. Nat Struct Mol Biol. 2007; 14:904–911. [PubMed: 17891149]
47. Jeschke G, Chechik V, Ionita P, Godt A, Zimmermann H, Banham J, Timmel C, Hilger D, Jung H. DeerAnalysis2006—a comprehensive software package for analyzing pulsed ELDOR data. Applied Magnetic Resonance. 2006; 30:473–498.

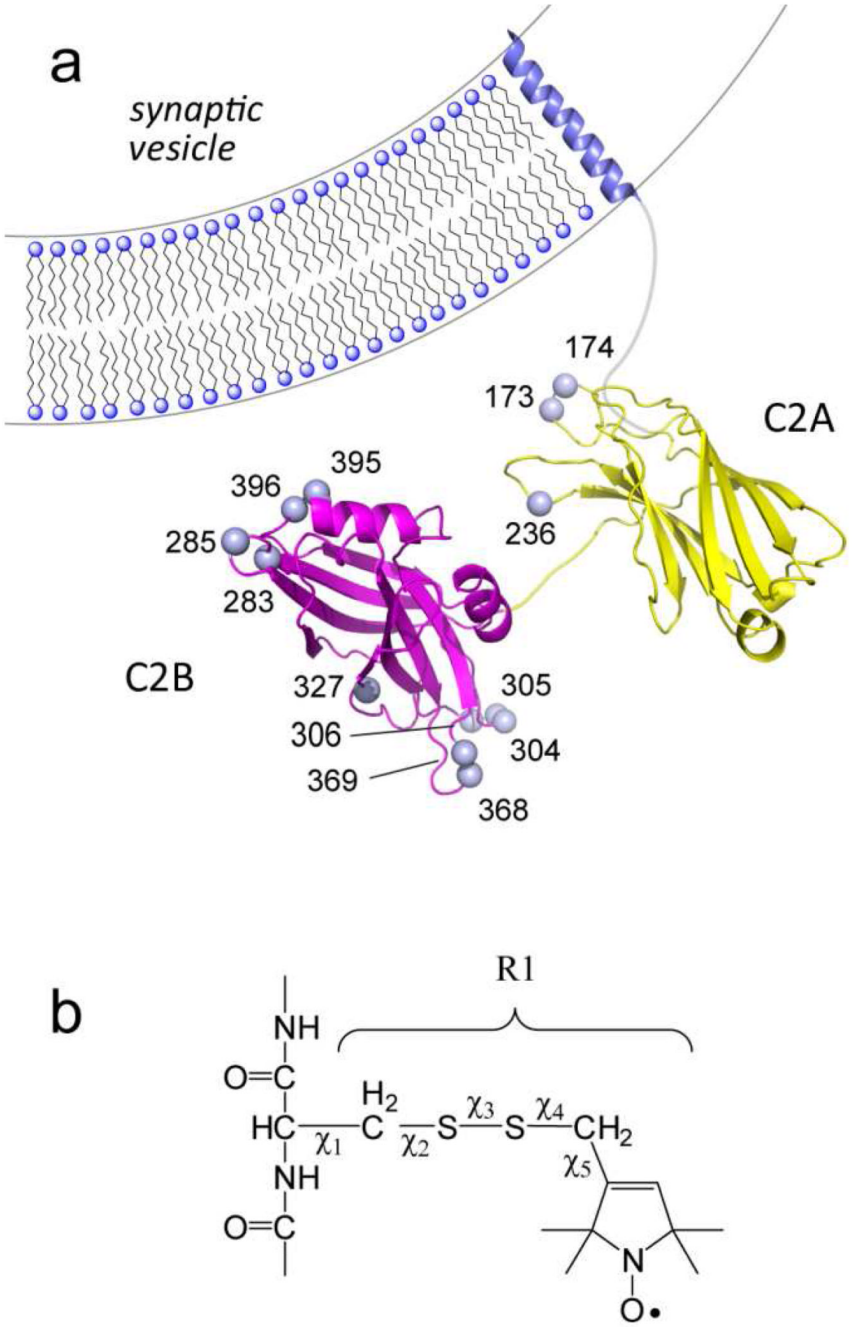

Figure 1.

a) Synaptotagmin 1 is a vesicle anchored protein containing two C2 domains (C2A, yellow and C2B, magenta). The membrane bound conformation of a soluble fragment of synaptotagmin 1 containing its two C2 domains, syt1C2AB, was determined in the presence of 1 mol% PIP_2. The spheres represent Cα carbons for positions that have been derivatized with the spin-labeled side chain R1. **b**) spin-labeled side chain R1 that is obtained derivatization of a cysteine residue with a methanethiosulfonate label.

Figure 2.

X-band EPR spectra obtained from single R1 substitutions in syt1 C2AB in the presence of Ca^{2+}. Spectra shown in black are in the presence of POPC:POPS (3:1) lipid vesicles, and spectra shown in red are in the presence of POPC:POPS:PIP_2 (74:25:1) lipid vesicles. Spectra are normalized against the total spin number so that the amplitudes provide an approximate measure of the motional averaging of the R1 side chain. All the spectra are 100 Gauss scans.

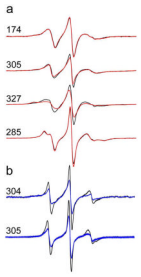

Figure 3.

a) Comparison of EPR spectra for several sites in syt1C2AB when bound to bilayers containing POPC:POPS with the addition of 1 mol% (black) and 5 mol% PIP_2 (red). **b**) EPR spectra in the absence of Ca^{2+} for two sites in syt1C2AB within the first Ca^{2+}-binding loop C2B when bound to either POPC:POPS (black) or POPC:POPS:PIP_2 bilayers (blue). Spectra are normalized against the total spin number and are 100 Gauss scans.

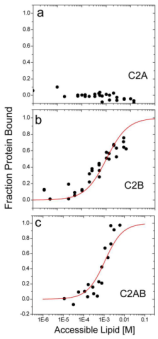

Figure 4.

Ca^{2+}-independent partitioning of **a**) C2A, **b**) C2B and **c**) C2AB to POPC:POPS:PIP_2 (74:25:1) bilayers determined by sedimentation equilibrium. The red traces represent fits to the data using equation 3. No binding of C2A in the absence of Ca^{2+} is detected to POPC:POPS:PIP_2 bilayers. Reciprocal molar partition coefficients obtained from these data are shown in Table 3.

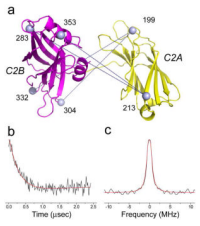

Figure 5.

Pulse EPR (DEER) was used to measure distances between the C2A and C2B domains of syt1C2AB when bound to POPC:POPS:PIP_2 bilayers. Shown in **a**) are sites for four spin labeled pairs used for distance measurements. The black traces in **b**) and **c**) represent the background subtracted DEER signal and Pake pattern obtained for the 199R1/304R1 spin pair. The red trace represents the fit to the data using a single Gaussian distribution, which is described by the mean distances and one standard deviation from the mean given in Table 3.

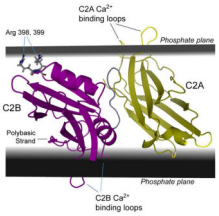

Figure 6.

Model for the membrane bound state of syt1C2AB when bound to POPC:POPS:PIP_2 (74:25:1) bilayers. The EPR-derived restraints could not be satisfied by docking to a single bilayer, but require the calcium-binding loops of C2B (magenta) and C2A (yellow) to insert into opposing bilayers. A region close to two conserved arginine residues in C2B (398 and 399), which are opposite the Ca^{2+}-binding loops, is located in the bilayer interface and requires that C2B domain contacts both membrane interfaces.

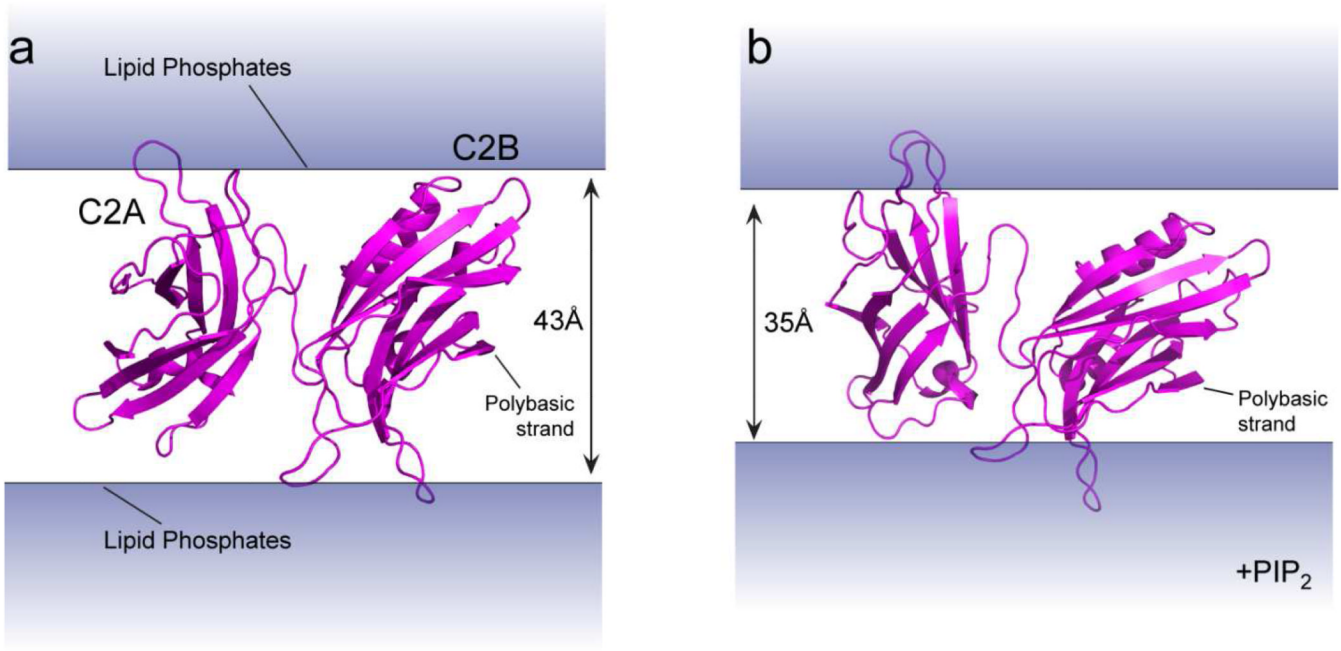

Figure 7.

Comparison of the models for membrane-bound syt1C2AB when associated with membrane vesicles composed of a) POPC:POPS (3:1) or b) POPC:POPS:PIP_2 (74:25:1). The addition of 1 mol% PIP_2 results in a model where the calcium binding loops of C2A and C2B are more deeply inserted, the polybasic strand of C2B is closer to the membrane interface, and the bilayer spacing that best fits the EPR-derived restraints is 5 to 8 Å less than that for POPC:POPS bilayers.

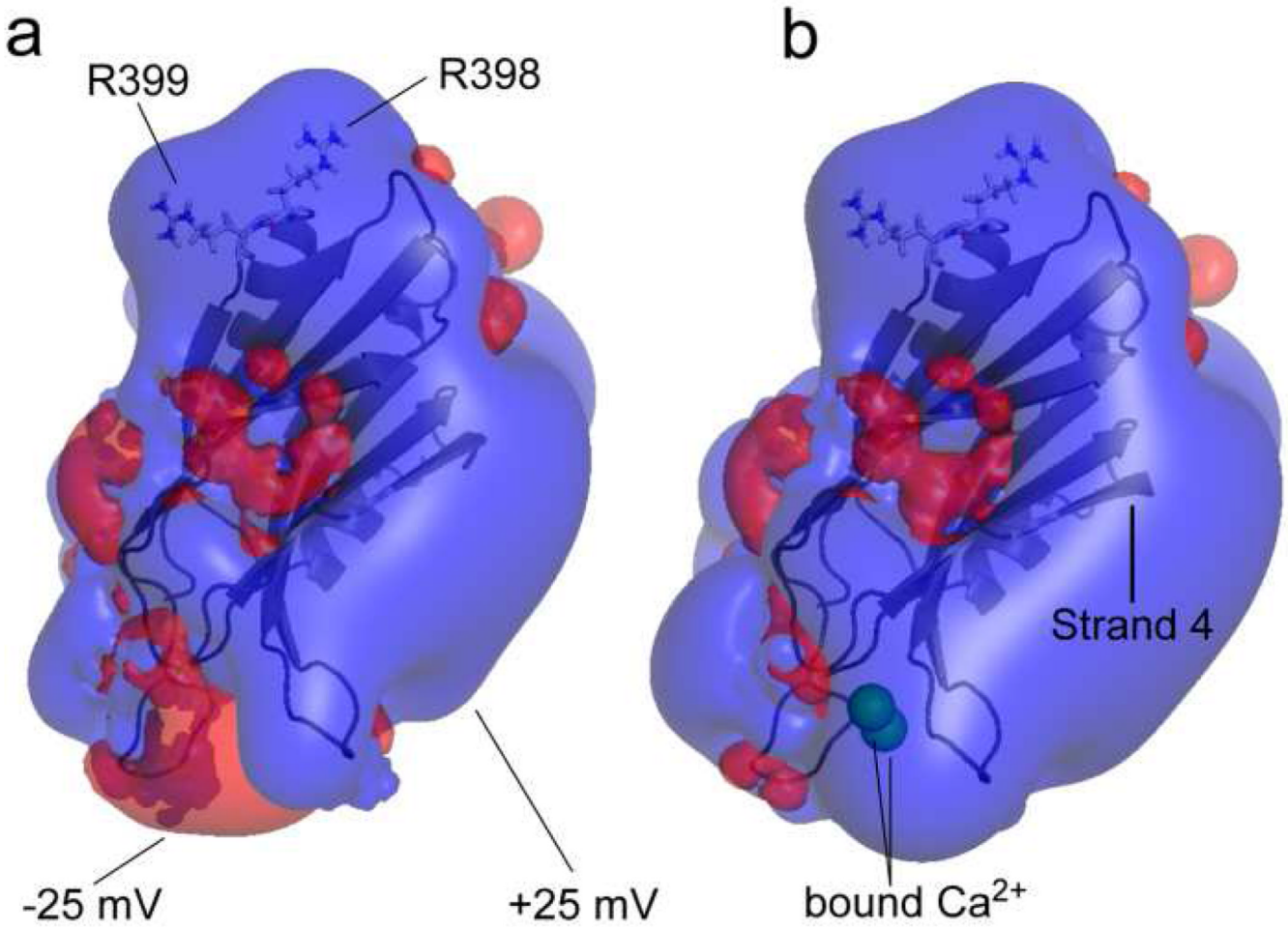

Figure 8.

Equipotential electrostatic surfaces (+25 mV, blue, −25 mV, red) for **a**) the C2B domain in the absence of Ca^{2+} and **b**) the C2B domain in the presence of Ca^{2+}. The C2B domain is highly positively charged, and has regions of positive charge due to its polybasic strand (strand 4) and highly conserved arginine residues located on a surface opposite the Ca^{2+}-binding loops. The binding of Ca^{2+} polarizes the primary membrane-binding face of the domain. The potentials were calculated using the APBS plug-in from PyMOL.

Table 1

Depth parameters, Φ, for spin labeled sites on syt1C2AB when associated with POPC:POPS (3:1) or POPC:POPS:PIP_2 (74:25:1) bilayers in the presence of calcium. The distances and range were calculated for PIP_2 containing bilayers. †

Labeled Site	Φ PC: PS	Φ (PC: PS: PIP_2)	Distance (Å)	Range (Å)
M173R1	0.8 ± 0.3	1.2 ± 0.3	+8.8	8.0 < × < 9.6
G174R1	0.6 ± 0.1	1.8 ± 0.2	+10.5	9.9 < × < 11.0
K236R1	−0.3 ± 0.2	1.2 ± 0.2	+8.8	8.2 < × < 9.3
V283R1	−1.9 ± 0.1	−2.2 ± 0.1	−10.6	−35.0 < × < −7.3
T285R1	−1.4 ± 0.1	−1.5 ± 0.1	−0.6	−1.3 < × < 0.0
V304R1	−0.4 ± 0.2	0.4 ± 0.3	+6.7	5.8 < × < 7.5
G305R1	0.8 ± 0.2	−1.1 ± 0.1	+1.6	1.1 < × < 2.0
G306R1	0.3 ± 0.3	0.2 ± 0.1	+6.1	5.8 < × < 6.4
K327R1	−2.2 ± 0.2	−1.7 ± 0.1	−2.1	−3.0 < × < −1.3
G368R1	0.6 ± 0.1	−0.9 ± 0.1	+2.4	0.6 < × < 3.9
K369R1	−1.2 ± 0.2	0.5 ± 0.2	+6.9	6.4 < × < 7.5
A395R1	−1.0 ± 0.1	−1.9 ± 0.1	−4.0	−5.4 < × < −3.0
N396R1	−2.1 ± 0.1	−1.4 ± 0.1	+0.0	−0.6 < × < 0.6

† Depth parameters were obtained by progressive power saturation of the EPR spectra and were used to estimate depths as described in Methods. The range was determined by uncertainty in the measured values of Φ and Eq. 1.

Table 2

Calcium independent reciprocal molar partition coefficients for syt1 C2B and C2AB to PC:PS (3:1) or PC/PS/PIP_2 (74:25:1) membranes[†]

	C2A	C2B	C2AB
PC:PS:PIP_2	-	$9.6(\pm1.1) \times 10^2$	$9.1(\pm1.6) \times 10^2$
PC:PS	-	$2.9(\pm0.3) \times 10^2$	$1.2(\pm0.1) \times 10^2$

[†]Partition coefficients determined by sedimentation (see Methods) in the presence of 1 mM EGTA. Partition coefficients to PC:PS in the absence of Ca^{2+} are shown for comparison and were published previously (13).

Table 3

Distances and distance distributions obtained by double electron-electron resonance (DEER) between spin labeled sites in C2A and C2B[†]

C2A/C2B mutant	POPC:POPS (3:1)	POPC:POPS:PIP_2 (74:25:1)
R199R1 / V304R1	40±14 (Å)	39 ± 16 (Å)
R199R1 / K332R1	46+8	52 ± 11
K213R1 / V283R1	61+16	56 ± 12
K213R1 / Q353R1	56+15	53 ± 15

[†]Measurements were made in the presence of Ca^{2+} (see methods). Distances were obtained by a Gaussian fit to the distance distribution using the program DEER Analysis 2009 (47). The distances represent the most populated distance and the range represents one standard deviation of the Gaussian distribution. The two shorter mutant pairs have approximately a 2 Å distance uncertainty and a 30% uncertainty in the distribution. For the two distances over 50 Å there is approximately a 4 Å distance uncertainty and a 50% uncertainty in the distribution. Data for POPC:POPS was obtained previously (23) and is shown here for comparison.